Beneficent features of Green's function with viscous effect

Xiaobo Chen and **Young-Myung Choi**

Research Department, Bureau Veritas Marine & Offshore, Paris, France

xiaobo.chen@bureauveritas.com

The new analysis further to the presentation of the ship-motion Green's function with viscous effect in [1] reveals several interesting features including the heavy damping to short waves, the removal of singularities in the vicinity of the source track and that across the critical frequency, and the smoothness of integrand functions. In particular, the effect of viscous coefficient on the integration of Green's function is studied.

1 Ship-motion Green's function with viscous effect

Within the classical reference system moving at the same speed U as the ship of length L, and using the basic parameters $(F, f, \tau) = (U/\sqrt{gL}, \omega\sqrt{L/g}, U\omega/g)$ associated with ω the encounter frequency and g the acceleration due to gravity, the fundamental solution to time-harmonic ship-motion problems is written as

$$4\pi G(\boldsymbol{x}, \boldsymbol{\xi}) = -1/r + 1/r' + G^F(\boldsymbol{x}, \boldsymbol{\xi}) \tag{1}$$

in which r is the distance from the field point $\boldsymbol{x}(x, y, z)$ to the source point $\boldsymbol{\xi}(\xi, \eta, \zeta)$ and r' is that to the mirror soure point $\boldsymbol{\xi}'(\xi, \eta, -\zeta)$. The free-surface term $G^F(\boldsymbol{x}, \boldsymbol{\xi})$ is given by the Fourier representation

$$F^2 G^F(\boldsymbol{x}, \boldsymbol{\xi}) = \frac{1}{\pi}\int_{-\pi}^{\pi} \mathrm{d}\theta \int_0^{\infty} \frac{k}{\mathcal{D}(k, \theta)} \mathrm{e}^{kZ}\, \mathrm{d}k \tag{2}$$

with the speed-scaled Fourier variable k and

$$Z = v - \mathrm{i}w\,, \quad v = (z + \zeta)/F^2 \quad \text{and} \quad w = (x - \xi)\cos\theta/F^2 + (y - \eta)\sin\theta/F^2 \tag{3}$$

The denominator $\mathcal{D}(k, \theta)$ of the integrand function in (2) is the dispersion function associated with the boundary condition on the free surface (eq.16) in [2] derived from the analysis based on the linearized Navier-Stokes equation and Helmoholtz decomposition and written by

$$\mathcal{D}(k, \theta) = (k\cos\theta - \tau)^2 - k - \mathrm{i}4\epsilon(k\cos\theta - \tau)k^2 \tag{4}$$

The speed-scaled coefficient ϵ in (4) is defined by

$$\epsilon = \nu/\left(F^3\sqrt{gL^3}\right) = \nu g/U^3 \tag{5}$$

in which ν denotes the fluid kinematic viscosity. The coefficient ϵ may take approximate values

$$\begin{array}{rcccc} U(\mathrm{m/s}) = & 0.01 & 0.1 & 1 & 10 \\ \epsilon \approx & 10 & 0.01 & 10^{-5} & 10^{-8} \end{array} \tag{6}$$

according to (5). Since $O(U) \approx O(1)$ in most applications of ship motions, the values of $\epsilon \approx 10^{-5}$ or in a range of $\epsilon \approx 10^{-3} \sim 10^{-6}$ can be taken. One of important objectives of the present work is to study the effect of viscous coefficient to the Green's function and its integration on flat panels.

2 Complex wavenumbers

The complex dispersion equation by putting (4) equal to zero

$$\mathcal{D}(k, \theta) = 0 = -\mathrm{i}4\epsilon\cos\theta(k - k_1)(k - k_2)(k - k_3) \tag{7}$$

has three complex roots

$$k_{1,2,3}(\theta) = \kappa_{1,2,3}(\theta) + \mathrm{i}\mu_{1,2,3}(\theta) \tag{8}$$

with $\kappa_{1,2,3}$ and $\mu_{1,2,3}$ being the real and imaginary parts, respectively, varying with the polar angle θ.

Let's start with the special case of $F \neq 0$ but $f = 0$ (steady flow $\tau = 0$) for which we have

$$k_1^s = 0\,,\quad k_2^s = \kappa_2^s + \mathrm{i}\mu_2^s = \frac{2}{\cos^2\theta + \sqrt{\cos^4\theta - \mathrm{i}16\epsilon\cos\theta}}\,,\quad k_3^s = \kappa_3^s + \mathrm{i}\mu_3^s = \frac{\cos^2\theta + \sqrt{\cos^4\theta - \mathrm{i}16\epsilon\cos\theta}}{\mathrm{i}8\epsilon\cos\theta} \tag{9}$$

given by (eq.2.12) in [3]. At the limit of $\epsilon \to 0^+$, the wavenumber $k_2^s = 1/\cos^2\theta$ covers the case of Neumann-Kevin steady flow. The third wavenumber $|k_3^s| \to \infty$ so that its contribution is nil.

For a finite value of $\epsilon \neq 0$, the real part κ_3^s is negative and imaginary $|\mu_3^s| \approx O(1/\epsilon)$. The real $\kappa_2^s \approx 1/\cos^2\theta$ is close to the wavenumber of steady flow for $|\cos\theta| > \sqrt[3]{16\epsilon}$, but very different for $\sqrt[3]{16\epsilon} > |\cos\theta| \to 0$. For the sake of presentation, we like to define at $\tau = 0$

$$k_1^0 = k_0^s/\tau^2 = 1 + \mathrm{i}4\epsilon^f\,,\quad k_2^0 = \begin{cases} k_2^s\cos\theta & \text{for} \quad \theta \geq \pi/2 \\ k_3^s\cos\theta & \text{for} \quad \theta < \pi/2 \end{cases}\,,\quad k_3^0 = \begin{cases} k_3^s\cos\theta & \text{for} \quad \theta \geq \pi/2 \\ k_2^s\cos\theta & \text{for} \quad \theta < \pi/2 \end{cases} \tag{10}$$

with $\epsilon^f = \nu f^3/\sqrt{gL^3}$ in k_1^0 applying for $f \neq 0$ (zero-speed $\tau = 0$), and (k_2^0, k_3^0) for $F \neq 0$ (steady flow $\tau = 0$), and in general case of $\tau > 0$

$$k_1^\tau = k_1/\tau^2\,,\quad k_{2,3}^\tau = \kappa_{2,3}^\tau + \mathrm{i}\mu_{2,3}^\tau = k_{2,3}\cos\theta = \kappa_{2,3}\cos\theta + \mathrm{i}\mu_{2,3}\cos\theta \tag{11}$$

The cubic dispersion equation (7) can be solved by applying the Cardano's formulae to obtain three complex roots (8). The wavenumbers $(k_1^\tau, k_2^\tau, k_3^\tau)$ scaled by (11) are illustrated on the left, in the middle, and on the right of Figure 1, respectively. The real and imaginary parts are depicted against the value $\cos\theta$ for

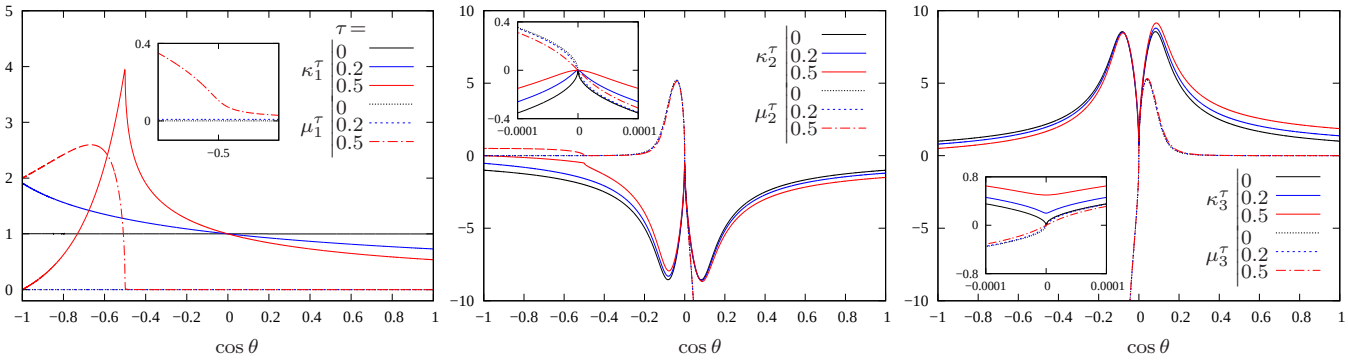

Figure 1: Wavenumber curves $(k_1^\tau, k_2^\tau, k_3^\tau)$ are illustrated against $\cos\theta$, on the left, in the middle and on the right.

$\theta \in (0, \pi)$, by the solid and dashed lines, respectively. With one value of $\epsilon = 10^{-4}$, three values of $\tau = 0$, 0.2 and 0.5 are used and associated wavenumber curves are painted in black, blue and red colors, respectively.

The wavenumber k_1^τ is of finite magnitude. Its real part κ_1^τ is very close to that of inviscid case and its imaginary part $\mu_1^\tau \approx \epsilon$ for $\tau \leq 1/4$. For $\tau > 1/4$, $\mu_1^\tau \approx \sqrt{-1/4 - \tau\cos\theta}/(\tau^2\cos^2\theta)$ for $\theta \geq \pi - \theta_c$ with $\theta_c = \arctan\sqrt{16\tau^2 - 1}$, but smoothly crossing $\theta = \theta_c$ as shown by the zoomed view. The wavenumbers k_2^τ and k_3^τ vary smoothly crossing $\theta = \pi/2$. Indeed, $k_2^\tau \approx O(\cos^2\theta)$ and $k_3^\tau \approx \tau + O(\cos^2\theta)$ for $\tau > 0$. Particularly at $\tau = 0$, $\kappa_2^0 = -\kappa_3^0 = -\sqrt{|\cos\theta|/(8\epsilon)}$. The wavenumber $k_2 = k_2^\tau/\cos\theta > 0$ for $\theta > \pi/2$ and $k_3 = k_3^\tau/\cos\theta > 0$ for $\theta < \pi/2$ are associated with wave components. On the other side, The wavenumber $\kappa_2 = \kappa_2^\tau/\cos\theta < 0$ for $\theta < \pi/2$ and $\kappa_3 = \kappa_3^\tau/\cos\theta < 0$ for $\theta > \pi/2$ are associated with evanescent local components, largely damped by the fact that $|\mu_2| \approx O(1/\epsilon)$ for $\theta < \pi/2$ and $|\mu_3| \approx O(1/\epsilon)$ for $\theta > \pi/2$. On the other side, the imaginary wavenumber $\mu_2 = \mu_2^\tau/\cos\theta \approx -\mu_1$ for $\theta > \theta_c$ and smoothly crosses $\theta = \theta_c$.

3 Integration of Green's function over panels

Introducing (7) into (2) and using the fraction decomposition of $k/\mathcal{D}(k,\theta)$, we have

$$F^2 G^F(\boldsymbol{x},\boldsymbol{\xi}) = \frac{1}{\pi}\int_{-\pi}^{\pi}\left[A_1(\theta)K(\boldsymbol{x},\boldsymbol{\xi},k_1) + A_2(\theta)K(\boldsymbol{x},\boldsymbol{\xi},k_2) + A_3(\theta)K(\boldsymbol{x},\boldsymbol{\xi},k_3)\right]\mathrm{d}\theta \tag{12}$$

with the complex amplitude functions $A_n(\theta)$ for $n = 1, 2, 3$ which are associated with the fraction decomposition and given by

$$\begin{aligned} A_1(\theta) &= \mathrm{i}k_1/[4\epsilon\cos\theta(k_1-k_2)(k_1-k_3)] \\ A_2(\theta) &= \mathrm{i}k_2/[4\epsilon\cos\theta(k_2-k_3)(k_2-k_1)] \\ A_3(\theta) &= \mathrm{i}k_3/[4\epsilon\cos\theta(k_3-k_1)(k_3-k_2)] \end{aligned} \tag{13}$$

The functions $K(\boldsymbol{x}, \boldsymbol{\xi}, k_n) = K(v - \mathrm{i}w, \kappa_n + \mathrm{i}\mu_n)$ for $n = 1, 2, 3$ with (v, w) defined by (3) represent the inner k-integrals associated with $k_n = \kappa_n + \mathrm{i}\mu_n$ written by :

$$K(Z,k) = \int_0^\infty \frac{\mathrm{e}^{t(v-\mathrm{i}w)}}{t-(\kappa+\mathrm{i}\mu)}\,\mathrm{d}t = \mathrm{e}^{kZ}E_1(kZ) + \mathrm{i}\pi\left[\mathrm{sgn}(\mu)+\mathrm{sgn}(\mu v-\kappa w)\right]H(\kappa)\mathrm{e}^{kZ} \tag{14}$$

in which $Z = v - \mathrm{i}w$, and $k = \kappa + \mathrm{i}\mu$, $E_1(\cdot)$ is the exponential-integral function defined by (eq.5.1.1) in [4], $\mathrm{sgn}(\cdot)$ the sign function and $H(\cdot)$ the Heaviside function. This special wavenumber-integral function $K(\cdot)$ expressed analytically by (14) can then be evaluated accurately by using numerical algorithms for the exponential-integral function. Furthermore, the integration of $K(\cdot)$ over a flat panel can be performed in an analytical way.

Considering a flat panel h_q of polygonal form with m_q vertices with the coordinates $Q_j(\xi_j, \eta_j, \zeta_j)$ for $j = 1, 2, \cdots, m_q$, and connectivities from Q_j to Q_{j+1} with $Q_{m_{q+1}} = Q_1$ to close the contour, the normal vector is denoted as $\boldsymbol{n} = (n_1, n_2, n_3)$ according to the right-hand-thumb rule. The integration of the wavenumber-integral function is written by

$$\mathcal{K}(\boldsymbol{x}, h_q, k) = \iint_{h_q} K(Z,k)\,\mathrm{d}S(\boldsymbol{\xi}) = k^{-1}\sum_{j=1}^{m_q}\left\{(k^{-1}c_j + d_j)\big[K(k,Z_j) + \ln(-Z_j)\big] + c_j R(Z_j)\right\} \tag{15}$$

obtained in [5] by applying Stokes' theorem to transform an integral on panel surface to contour integrals along the panel's sides. In (15), $k = \kappa + \mathrm{i}\mu$ representing the complex wavenumbers k_n for $n = 1, 2, 3$ and the functions

$$\begin{aligned} R(Z_j) &= Z_j\ln(-Z_j) - Z_j \\ F^2 Z_j &= z + \zeta_j - \mathrm{i}[(x-\xi_j)\cos\theta + (y-\eta_j)\sin\theta] \end{aligned} \tag{16}$$

are used with the coefficients (c_j, d_j) defined by

$$\begin{aligned} F^2 c_j &= (n_2+\mathrm{i}n_3\sin\theta)\big[(\xi_j-\xi_{j-1})\delta^c_{j-1} - (\xi_{j+1}-\xi_j)\delta^c_j\big] - (n_1+\mathrm{i}n_3\cos\theta)\big[(\eta_j-\eta_{j-1})\delta^c_{j-1} - (\eta_{j+1}-\eta_j)\delta^c_j\big] \\ F^2 d_j &= (n_2+\mathrm{i}n_3\sin\theta)\big[(\xi_j-\xi_{j-1})\delta^d_{j-1} + (\xi_{j+1}-\xi_j)\delta^d_j\big] - (n_1+\mathrm{i}n_3\cos\theta)\big[(\eta_j-\eta_{j-1})\delta^d_{j-1} + (\eta_{j+1}-\eta_j)\delta^d_j\big] \end{aligned} \tag{17}$$

and (δ^c_j, δ^d_j) given by

$$\delta^c_j = \begin{cases} 1/\chi_j & \text{for } |\chi_j| > 0 \\ 0 & \text{for } |\chi_j| = 0 \end{cases} \quad \text{and} \quad \delta^d_j = \begin{cases} 0 & \text{for } |\chi_j| > 0 \\ 1/2 & \text{for } |\chi_j| = 0 \end{cases} \tag{18}$$

$$\text{with } F^2\chi_j = \zeta_{j+1} - \zeta_j + \mathrm{i}[(\xi_{j+1}-\xi_j)\cos\theta + (\eta_{j+1}-\eta_j)\sin\theta]$$

for $j = 1, 2, \cdots, m_q$. It worth noting that the subscript sequence $(\cdot)_0 = (\cdot)_{m_q}$ and $(\cdot)_{m_q+1} = (\cdot)_1$ in applying (17). The coefficients (c_j, d_j) depend only on the geometry of panel h_q. The functions $\mathcal{K}(k, Z_j)$ has finite values for $Z_j \to 0$. The same for auxiliary functions $\mathcal{R}(Z_j)$ when $Z_j \to 0$. For large values of Z_j, alternative formulae are developed for $C(\boldsymbol{x}, k)$ well suit for its numerical evaluation. The integrations of the Green's function defined by (2) are then

$$\mathcal{G}^F(\boldsymbol{x}, h_q) = F^2\iint_{h_q} G^F(\boldsymbol{x},\boldsymbol{\xi})\mathrm{d}S(\boldsymbol{\xi}) = \frac{1}{\pi}\int_{-\pi}^{\pi}\big[A_1(\theta)\mathcal{K}(\boldsymbol{x},h_q,k_1) + A_2(\theta)\mathcal{K}(\boldsymbol{x},h_q,k_2) + A_3(\theta)\mathcal{K}(\boldsymbol{x},h_q,k_3)\big]\mathrm{d}\theta \tag{19}$$

reduced to single θ-integrals which can be evaluated numerically. According to (18), the coefficients d_j defined in (17) is negligible except in the vicinity of two critical θ-values at which, $w_j = 0$, the wavenumber vector parallel to $(\cos\theta, \sin\theta)$ is orthogonal to the direction in parallel to the segment Q_j-to-Q_{j+1} of panel h_q when both Q_j and Q_{j+1} are located at the same level (i.e. $\zeta_j = \zeta_{j+1}$). However, ignoring d_j can lead to significant numerical errors.

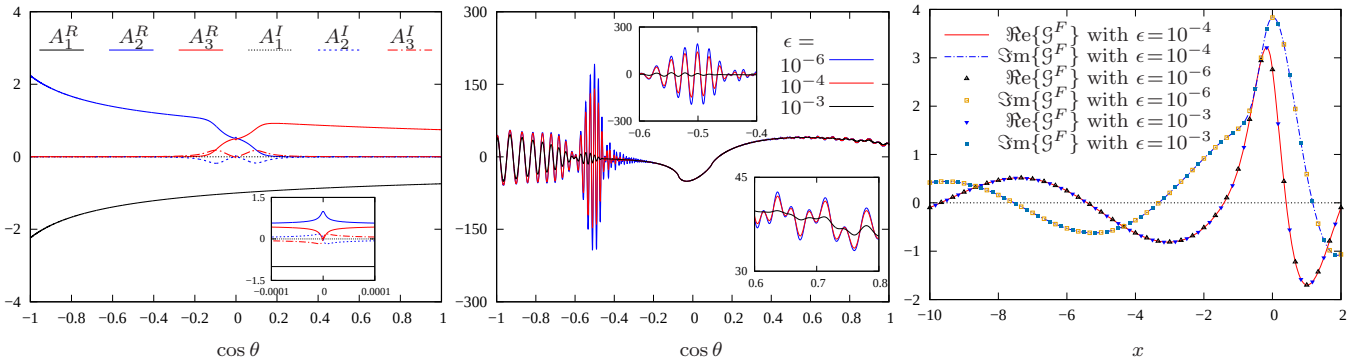

Figure 2: Amplitude functions (13) on the left and the integrand function in (19) in the middle against $\cos\theta$, and the integration of Green's function (19) on the right along the straight line $(x, 0, 0)$ over a vertical panel.

4 Discussion and conclusions

The complex amplitude functions $A_{1,2,3} = A^R_{1,2,3} + \mathrm{i}A^I_{1,2,3}$ defined by (13) associated with the complex wavenumbers $k_{1,2,3}$ the roots of the dispersion equation (7) are illustrated on the left of Figure 2 for $\tau = 0.2$ and $\epsilon = 10^{-4}$. The complex amplitude functions are smooth in the whole range of $|\cos\theta| \leq 1$ even in the vicinity of $\theta = \pi/2$ as shown by the zoom box. Due to the fact that the minimum $|\nabla\mathcal{D}| = 5\epsilon/4$ for $\tau = 1/4$, the amplitude functions (A_1, A_2) are of finite for $\tau = 1/4$ and $\tau > 1/4$ at $\theta = \theta_c$ in general.

A flat panel with 4 vertices $Q_1 = (-\sqrt{3}/4, -1/4, 0)$, $Q_2 = (-\sqrt{3}/4, -1/4, -1/2)$, $Q_3 = (\sqrt{3}/4, 1/4, -1/2)$ and $Q_4 = (\sqrt{3}/4, 1/4, 0)$ is used as an example to integrate the wavenumber-integral function. The integrand function in (19) is depicted for a field point $\boldsymbol{x} = (-3, 0, 0)$ and represented in the middle of Figure 2. Three values of the viscous coefficient $\epsilon = 10^{-3}, 10^{-4}$ and 10^{-6} are used. The oscillatory integrand function is manifestly different for different values of viscous coefficient. The θ-integral (19) of the oscillatory integrand functions yields the value of integration of Green's function $\mathcal{G}^F(\boldsymbol{x}, h_q)$ on the flat panel, depicted on the right of Figure 2. It is shown the result is not sensitive to the viscous coefficient, as expected.

The viscous effect is introduced through the analysis of real fluid flow based on the linearised Navier-Stokes equation and Helmholtz decomposition in [2], and resultant Green's function possesses many interesting features. First, the dispersion equation becomes complex and has three complex wavenumbers instead of two real roots if viscosity is nil. The short-length divergent waves are deformed and highly damped due to the presence of viscosity. Second, at the critical frequency corresponding to $\tau = 1/4$, the Green's function is of finite value and should provide results with a smooth transition crossing the critical frequency. Third, the integrand function in the Fourier representation becomes smooth where it is sharp variation or singular if viscosity is absent, and less oscillatory due to damping effect. Furthermore, the analytical integration over flat panels including those on the free surface provides the accurate elements of the boundary integral equations, which are few affected by the viscous coefficient used. Indeed, the recent development based on new boundary integral equations involving the integration of Green's function over the free surface in the vicinity of ship hull, presented in [5] shows the excellent agreement of final results (added-mass and damping coefficients) with measurements of model tests. This confirms the soundness of Green's function with viscosity and its beneficent features.

References

[1] Chen XB, Liang H & Choi YM (2020) Ship-motion Green function with viscosity effect. *Proc. 35th IWWWWFB*. Seoul, Korea.

[2] Chen XB & Dias F (2010) Visco-potential flow and time-harmonic ship waves. *Proc. 25th IWWWWFB*. Harbin, China.

[3] Liang H & Chen XB (2019) Viscous effects on the fundamental solution to ship waves. *J. Fluid Mech.*, 879, 744-774.

[4] Abramowitz M & Stegun IA (1967) Handbook of mathematical functions. *Dover publications*.

[5] Chen XB, Choi YM, Malenica S & Derbanne Q (2020) Ecoulement instationnaire sur le courant dévié par navire. *Actes des 17èmes Journées de l'Hydrodynamique*. Cherbourg-en-Cotentin, France.